Journal of Hydrology 523 (2015) 624–635

Contents lists available at ScienceDirect

Journal of Hydrology

journal homepage: www.elsevier.com/locate/jhydrol

Recent and old groundwater in the Niebla-Posadas regional aquifer (southern Spain): Implications for its management

Laura Scheiber [a,*], Carlos Ayora [a], Enric Vázquez-Suñé [a], Dioni I. Cendón [b,c], Albert Soler [d], Emilio Custodio [e], Juan Carlos Baquero [f]

[a] Institute of Environmental Assessment and Water Research, CSIC, Jordi Girona 18, E-08034 Barcelona, Spain
[b] Australian Nuclear Science and Technology Organisation, Locked Bag 2001, Kirrawee DC, NSW 2232, Australia
[c] School of Biological, Earth and Environmental Sciences (BEES), University of New South Wales (UNSW), Sydney, NSW 2052, Australia
[d] Departament de Cristal·lografia, Mineralogia i Dipòsits Minerals, Facultat de Geologia, Universitat de Barcelona, C/Martí Franquès, sn, Barcelona, Spain
[e] Department of Geo-Engineering, Technical University of Catalonia (UPC), Barcelona, Spain
[f] Cobre Las Cruces S.A., Carretera SE-3410 km 4, 41860 Gerena, Sevilla, Spain

ARTICLE INFO

Article history:
Received 23 October 2014
Received in revised form 22 January 2015
Accepted 30 January 2015
Available online 11 February 2015
This manuscript was handled by Laurent Charlet, Editor-in-Chief, with the assistance of Rafael Pérez-López, Associate Editor

Keywords:
Niebla-Posadas aquifer
Groundwater residence time
^{13}C sinks and sources
Environmental isotopes
Groundwater sustainability

SUMMARY

The Niebla-Posadas (NP) aquifer in southern Spain is one of the main groundwater sources for the lower Guadalquivir Valley, a semiarid region supporting an important population, agriculture and industry. To contribute to the understanding of this aquifer the assessment of sustainable use of groundwater, the residence time of groundwater in the NP aquifer has been estimated using ^{3}H, ^{14}C and ^{36}Cl. Along the flow paths, recharged groundwater mixes with NaCl-type waters and undergoes calcite dissolution and is further modified by cation exchange (Ca–Na). Consequently, the water loses most of its calcium and the residual $\delta^{13}C_{DIC}$ in the groundwater is isotopically enriched. Further modifications take place along the flow path in deeper zones, where depleted $\delta^{13}C_{DIC}$ values are overprinted due to SO_4^{2-} and iron oxide reduction, triggered by the presence of organic matter. Dating with ^{3}H, ^{14}C and ^{36}Cl has allowed the differentiation of several zones: recharge zone (<0.06 ky), intermediate zone (0.06–20 ky), deep zone 1 (20–30 ky), and deep zone 2 (>30 ky). An apparent link between the tectonic structure and the groundwater residence time zonation can be established. Regional faults clearly separates deep zone 1 from the distinctly older age (>30 ky) deep zone 2. From the estimated residence times, two groundwater areas of different behavior can be differentiated within the aquifer.

1. Introduction

With a surface of 60,000 km^2, the Guadalquivir basin is a major geological and hydrological unit in southern Spain, sustaining a population of more than 4 million. It is a semiarid region where the distribution of water resources between human use and the environment is a challenge (CHG, 2012). The Niebla-Posadas (NP) aquifer is one of the main groundwater resources of the lower Guadalquivir basin. It supports traditional agriculture and is a drinking water reserve for many localities, including Seville. Further competition for water resources in recent years in the area has arisen from the expansion of irrigation agriculture, with an increase of 64% of irrigated crop area in the 2000–2011 period (CHG, 2012), gas explorations and the opening of two major open-pit mines. The Cobre Las Cruces (CLC) and Aznalcollar mines (now in the process of reopening after a serious environmental incident about 15 years ago) exploit ore bodies located in contact with the base of the Niebla-Posadas (NP) aquifer. The CLC mining complex is one of the largest open pit mining in Europe. To drain the open pit, a world-class Drainage and Reinjection System (DRS) has been implemented. The DRS is formed by two rings of perimetral wells, one of drainage wells and the other of reinjection wells. The function of this system is to prevent groundwater head drawdown and pollution of the NP aquifer outside the mining project. Farther to the south, the deeper NP sands below the Doñana National Park (>2000 m depth) host gas reserves and the feasibility of temporary CO_2 storage in the sands has been studied.

In NP aquifer, groundwater salinity increases with depth following a characteristic pattern discussed by Tóth (1999), common in many aquifers worldwide (e.g.: Frengstad et al., 2001; Wen et al., 2005; Cloutier et al., 2006; Su et al., 2013; and many others). Furthermore, the complex regional geological structure complicates the identification of flow paths and the assessment of tracer travel

* Corresponding author. Tel.: +34 934006100; fax: +34 932045904.
E-mail address: scheiber.ls@gmail.com (L. Scheiber).

http://dx.doi.org/10.1016/j.jhydrol.2015.01.076
0022-1694/

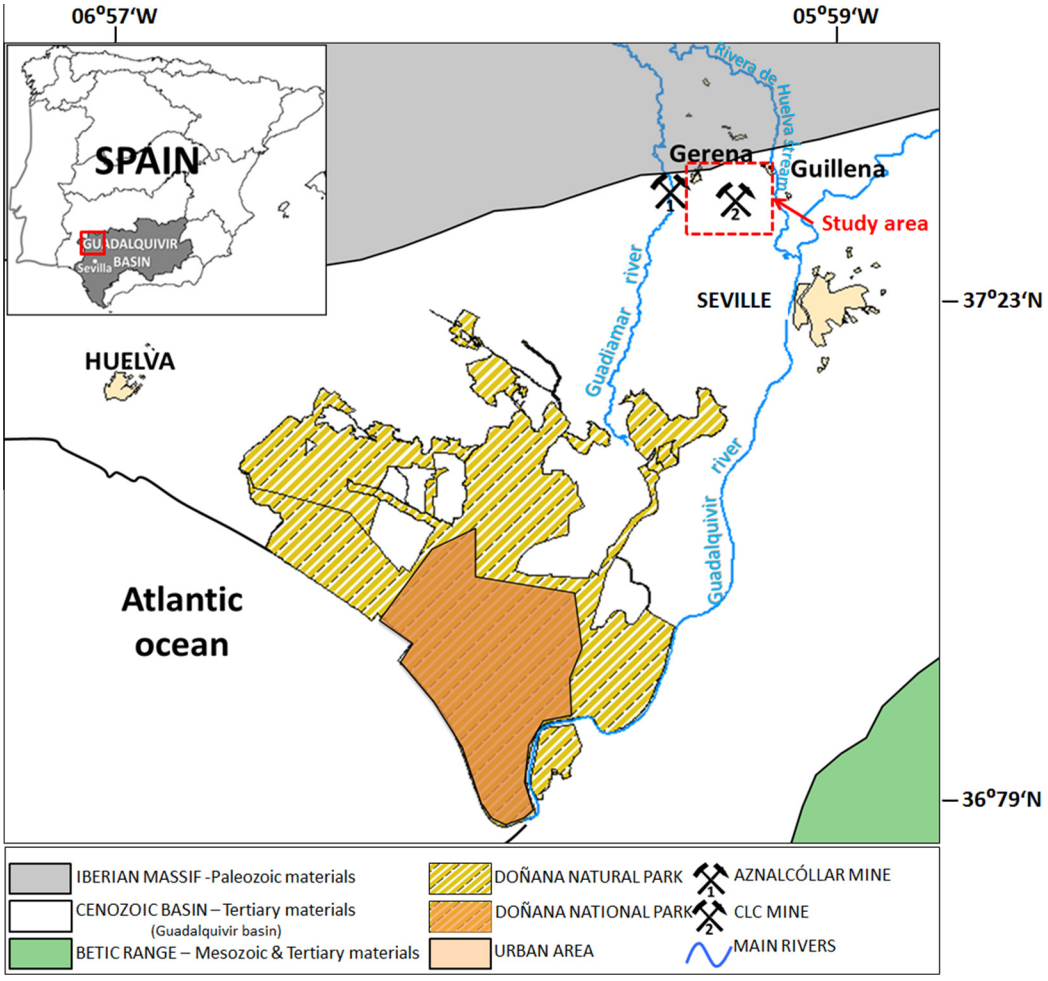

Fig. 1. Regional map with major catchments boundaries and detail of main regional relief units.

times. The consequence is a multiple hydraulic and hydrochemical zonation. All these considerations result in a highly complex hydrogeochemical zonation of the NP aquifer. This generates groundwater management uncertainties that include key issues such as the definition of uses, reserves estimation, water quality degradation induced by mixing and pumping, etc. In summary, the increasing demand for mining and agriculture and the rising public opinion concerns require a clearer assessment of groundwater.

Despite the described setting, no scientifically based assessment of water reserves is available. To respond to these questions, a hydraulic and hydrogeochemical conceptual model is needed. The objective of the present work is to define a methodology based on a combination of hydrogeochemical and isotopic techniques to identify which part of the aquifer contains groundwater that can be regarded as a renewable resource and which part is mostly composed of fossil groundwater. This will enhance the understanding of the groundwater system dynamics and become a support for sustainable management and protection of groundwater resources, which likely can be generalized to other similar studies.

To achieve the defined objective, a hydrogeochemical and groundwater dating study has been carried out. The use of hydrochemistry and environmental isotopes is an effective method to differentiate water–rock interactions and define the origin of groundwater, in order to construct a conceptual model of transfer processes between different aquifer waters (Dogramaci and Herczeg, 2002; Edmunds et al., 2002; Andre et al., 2005; Edmunds, 2009; Cartwright et al., 2010; among many others). Moreover, residence time estimation will be used, employing radioisotopes such as ^{3}H, ^{14}C, ^{36}Cl. This will be crucial to identify the volumes of non-renewable groundwater. A number of studies have used radioisotopes (^{3}H, ^{14}C, ^{36}Cl) to identify ancient and modern recharge and to estimate time scales of groundwater renewal (Bentley et al., 1986; Guendouz and Michelot, 2006; Cartwright et al., 2012; Meredith et al., 2012; Plummer et al., 2012; Cendón et al., 2014).

Some recent works also combine hydrogeochemical and isotopic techniques to estimate recharge sources and residence times to assess the sustainability of regional aquifer water resources development (Bouchaou et al., 2008; Mahlknecht et al., 2006; Sukhija et al., 2006; Douglas et al., 2007; Cresswell et al., 2001; Wallin et al., 2005; Currell et al., 2013; Atkinson et al., 2013). The recent proliferation of mining activities foreseeably makes these techniques the most likely immediate application of the methodology and conclusions of the present paper.

2. Hydrogeological setting

The Guadalquivir depression was formed during the Neogene due to the compression of Africa against Eurasia. It constitutes a foreland basin located between an active edge, the Betic Range, and the passive edge of the old Iberian (Hesperian) Massif (Fig. 1). The northern margin of the Guadalquivir Basin is in contact with

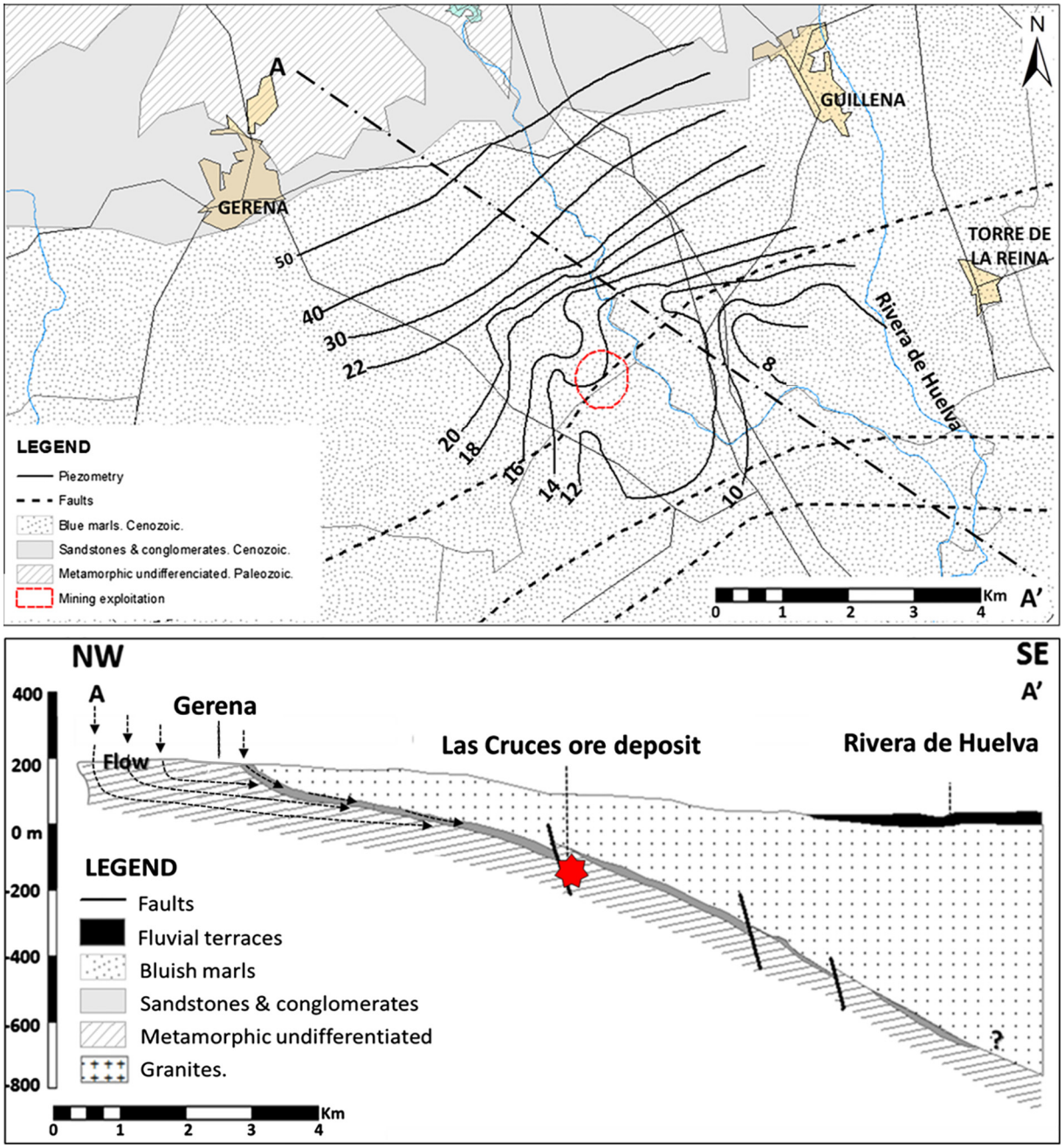

Fig. 2. Geological map with piezometric contour lines before mine operation, in metres above mean sea level and generalized cross section AA′.

materials in the Hesperian Massif; it is known as the South Portuguese area. This area is formed by Paleozoic rocks that form the base of Cenozoic and Quaternary materials that fill the Guadalquivir basin in its passive margin. Geologically, it consists of three major stratigraphic units defined for the whole South Portuguese area according to the dominat lithology: slates and quartzites group, volcano-sedimentary complex, and Culm Group (Blake (2008), Capitán Suárez (2006) and Fernández-Caliani and Galán (1991)).

The study area is located in the northern edge of the Guadalquivir basin, in the South Portuguese area, approximately 20 km north of Seville. The area limits are the Guadiamar River and Aznalcollar mine to the west and the Rivera de Huelva stream to the east, and include the CLC open pit mine (Fig. 1). The northernmost margin is marked by contact with the reliefs of Sierra Morena and the southern boundary by the Cortijuelos Creek.

The climate is temperate-warm Mediterranean due to the influence of the Atlantic Ocean and the Sierra Morena range elevations. Annual precipitation is 500–600 mm/y with an irregular intra-annual and inter-annual pattern. Current average yearly temperatures are 9–10 °C in mountainous areas and 15–18 °C in the valley region.

The study area is mostly covered by Quaternary materials associated with river deposits. Underlying Cenozoic bluish marls of marine origin form a wedge that thickens toward the south. Conglomerates, detrital limestones and sandstones with abundant marine microfauna form the base of the Cenozoic, which deepen southwards. The detrital materials outcrop on the northern margin of the basin and become confined below the bluish marls. The basement is made of Paleozoic materials forming a paleorelief, mostly composed of quartzite, schists, granite and volcanogenic

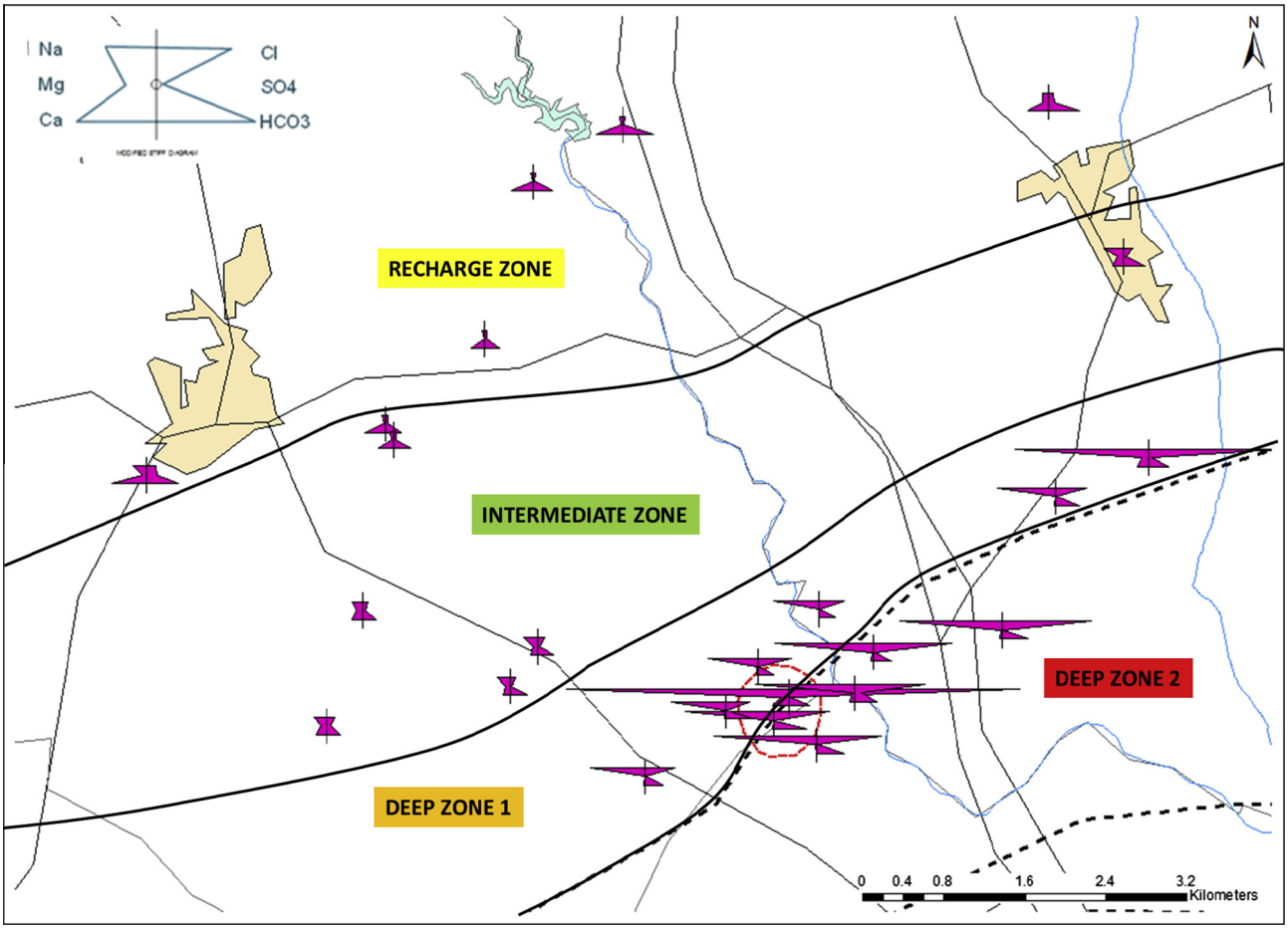

Fig. 3. Modified Stiff diagram showing the general chemistry of the groundwater samples and zonation of the study area according to geochemical and isotopic differences.

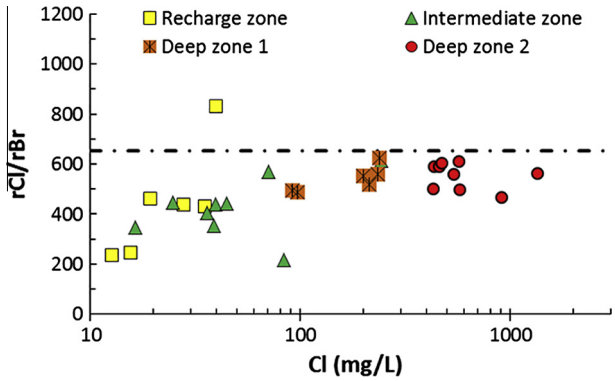

Fig. 4. Br–Cl molar ratios of analyzed groundwaters. Dashed line marks the marine Cl/Br ratio) Most of the analyzed samples plot along a line of continental values evolving toward more marine values as salinity increases (Whittemore, 1988; Davis et al., 1998; Herrera and Custodio, 2000; Alcalá and Custodio, 2008).

massive sulfide deposits. This basement is affected by a series of SW–NE oriented fractures and other less relevant NW–SE fractures (see Fig. 2).

The NP aquifer unit is formed by the detrital strata at the base of the Cenozoic formation. The aquifer is 10–30 m in thickness and gradually dips southward with a gentle slope (4–6%), being confined by the very low transmissivity marls (<5 m^2/d), up to 2000 m thick. The Paleozoic basement is fractured and weathered in its upper part, thus constituting a zone of relatively high permeability. The NP sandstone and the upper part of the basement underlying it define the relatively high transmissivity aquifer of the region. Transmissivity values range between 10 and 500 m^2/d and storage coefficient values are of the order of 10^{-2} in the unconfined zone and between 10^{-3} and 10^{-5} in the confined areas (CHG, 2012). Recharge of the NP aquifer takes place by rainwater infiltration in the northern outcropping area. Total estimated recharge in the outcropping narrow strip is 9 hm^3/y, and the main discharge is pumping, about 40 hm^3/y (CHG, 2012; Navarro et al., 1993). Groundwater regional flow, prior to mine operations, was dominantly northwest to southeast, following the topography, although there is an abnormal change of gradient in the area around the mine site. This anomaly is attributed to an elevation of the basement paleorelief, where the NP aquifer locally disappears and the marl layer rests directly on the Paleozoic (Fig. 2).

3. Sampling and analytical methods

3.1. Groundwater sampling

Groundwater level and physicochemical values were measured in 50 wells during two field campaigns. Samples for chemical and isotope analysis were collected at 42 points (Fig. 3). The majority of wells are screened within the NP aquifer, but others extract water from the Paleozoic aquifer and some extract water from both aquifers. The distribution of sampling points is as homogeneous as possible, but the area occupied by the mining activity has a higher density. Toward the south of the studied area, the number of wells is very limited due to the increasing depth of the aquifer (>200 m)

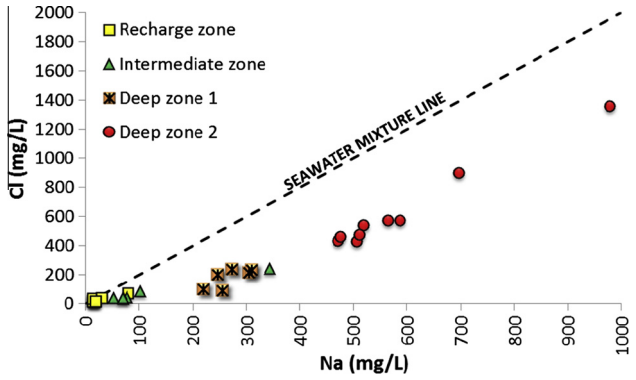

Fig. 5. Plot of Cl vs. Na in groundwater (values in mg/L).

and the declining groundwater quality. Before sampling, all wells were purged to remove three well volumes. Temperature (°C), specific electrical conductivity (SC, μS cm^{-1}), pH, Eh, and dissolved oxygen (DO, mg L^{-1}) were measured within a flow cell after reaching stability. Total alkalinity was determined in the field by acid-base titration using the Aquamerck Alkalinity Test.

3.2. Major/minor ions and gas analysis

Groundwater samples collected for general chemistry were filtered through a 0.22 μm nylon filter and collected in high-density polyethylene, 25 mL bottles for anions and 50 mL for cation-trace samples. The latter were acidified with 1 mL of 20% diluted nitric acid for sample preservation. Anions were analyzed by High Performance Liquid Chromatography (HPLC) and cations by Inductively Coupled Plasma Atomic Emission Spectrometry (ICP–AES), with an analytical error between 5% and 7.5%. A volume of 30 mL was collected for DOC (Dissolved Organic Carbon) analysis in glass bottles previously muffled. These samples were passed through a 0.45 μm nylon filter and acidified with 1 mL of HCl (2 N); the bottles were sealed with Parafilm® to minimize any contact with air. DOC was analyzed by the catalytic oxidation method at 680 °C using a Shimadzu TOC-V CSH instrument, with a detection limit of 0.05 mg/L. NH_4^+ was analyzed with a selective electrode Orion 9512, with an error of ±2%.

Twelve samples for gas (CH_4 and H_2S) analysis were collected in 250 mL glass bottles with septum cap and stored in an upside-down vertical position (Capasso and Inguaggiato, 1998). The CH_4 in the gas phase was determined using a Trace GC Ultra ThermoFisher Scientific chromatograph, with an analytical error from ±0.001 to ±0.009 mg/L and a detection limit of 0.58 mg/L. The CH_4 dissolved in water was obtained by the liquid gas partition coefficient. The H_2S content in the liquid phase was analyzed by ionic chromatography with a DIONEX model IC5000, and with a variable wavelength detector with a detection limit of 0.005 mg/L S_2 and an analytical error of 5%.

3.3. Stable isotopes $\delta^2H/\delta^{18}O$, $\delta^{34}S/\delta^{18}O$ in sulfate and $\delta^{13}C_{DIC}$

Water samples were collected for δ^2H and $\delta^{18}O$ analysis in 50 mL high-density polyethylene bottles. Samples for $\delta^{13}C_{DIC}$ were stored in 25 mL muffled glass bottles without headspace and sealed with Parafilm® to minimize any contact with air. All of them were filtered with 0.45 μm nylon filters. A Wavelength Scanned Cavity Ringdown Spectroscopy (WS-CRDS) instrument was used for δ^2H and $\delta^{18}O$ in water. A gas-bench system using the conventional H_3PO_4 method was used for $\delta^{13}C_{DIC}$ analysis (Torres et al., 2005). Isotopic results are given in δ notation against V-SMOW and V-PDB standards. The analytical precision is ±0.8‰ for δ^2H and ±0.3‰ for $\delta^{18}O$ and $\delta^{13}C_{DIC}$.

To determine $\delta^{34}S$ and $\delta^{18}O$ in sulfate, 2 L samples in polyethylene terephthalate (PET) bottles were collected, acidified with HCl, with an excess of barium chloride solution added to precipitate $BaSO_4$. The precipitation was carried out at elevated temperature (≈100 °C) to prevent the formation of $BaCO_3$. After settling, the precipitate was recovered by filtration through a 3-μm filter and dried at room temperature. The $\delta^{34}S_{SO4}$ was analyzed in a Carlo Erba Elemental Analyzer (EA) coupled in continuous flow to a Finnigan Delta C IRMS. $\delta^{18}O_{SO4}$ was analyzed in duplicate with a ThermoQuest TC/EA unit (high temperature conversion elemental analyzer) with a Finnigan Matt Delta C IRMS. The analytical error is 0.1–0.6 for $\delta^{34}S$ and 0.1–0.8 for $\delta^{18}O$.

3.4. Radioactive isotopes: ^3H, $^{14}C_{DIC}$ and ^{36}Cl

Samples for ^3H, $^{14}C_{DIC}$ and ^{36}Cl analysis were taken in 1 L glass bottles and after 0.45 μm filtration were sealed with Parafilm® to minimize any contact with air. The tritium (^3H) content of the samples was analyzed by liquid scintillation after electrolytic enrichment at the Universitat Autónoma de Barcelona (UAB). The ^3H concentrations are given in tritium units (TU) with a quantification limit of ±0.3 TU. The samples for ^{14}C were analyzed at the Australian Nuclear Science and Technology Organisation (ANSTO). For the analysis of ^{14}C, the dissolved inorganic carbon (DIC) was liberated from the samples with phosphoric acid as CO_2, which was captured using online extraction. The CO_2 was transformed quantitatively into graphite by reduction with hydrogen gas in

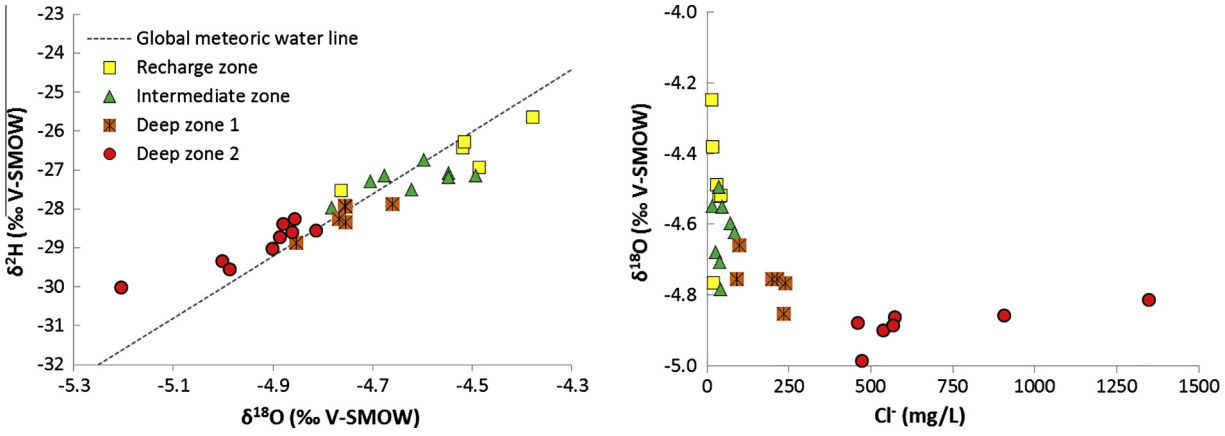

Fig. 6. $\delta^{18}O$ vs. $\delta\ ^2H$ content in groundwater and $\delta^{18}O$ vs. Cl.

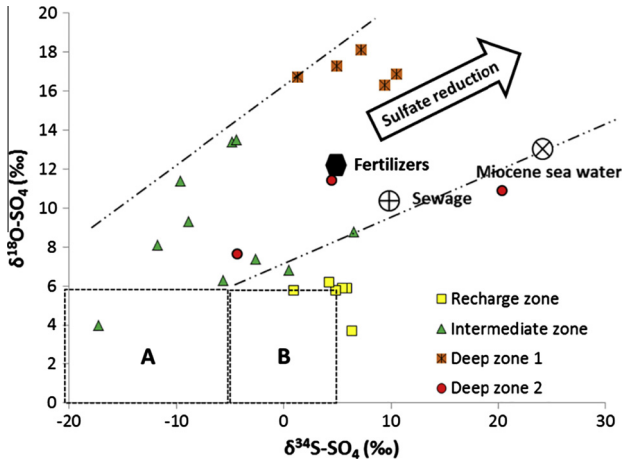

Fig. 7. Representation of the isotopic content of sulfates in groundwater. A: Sulfate derived from sedimentary sulfide oxidation. B: Sulfate derived from magmatic sulfide oxidation.

the presence of an iron catalyst. The ^{14}C activities were measured by accelerator mass spectrometry (AMS) using the 2MV ANSTO Tandetron accelerator STAR and expressed as a percentage of modern carbon (pMC) according to convention (Stuiver and Polach, 1977), with error ranging between ±0.03 and ±0.4. For ^{36}Cl determination, Cl^- was precipitated with silver chloride and then purified to minimize sulfur content. The precipitate was pressed into silver bromide masks in copper holders, and the ^{36}Cl isotope content of water samples was analyzed by the 14UD tandem accelerator at the Australian National University (Fifield et al., 1987). Analytical error ranged between ±1.7 and ±2.2 ($\times 10^{-15}$).

4. Results and discussion

4.1. General hydrochemistry

The study area has been divided into 4 zones: recharge, intermediate, and deep (1 and 2) zones. This zonation corresponds to geochemical and isotopic differences and clearly correlates with the main geological features (i.e., the principal faults), as explained below (Fig. 3).

Field determinations and complete chemical and isotopic data of each water sample are recorded in Table A1 of Supplementary information.

Groundwater temperatures range between 17.8 and 36.5 °C; the lowest values are for shallow groundwater in the recharge area while higher temperatures correspond to deep samples toward the southeast. A vertical temperature profile obtained along 80 m shows a high geothermal gradient of 12 °C/100 m, well above the average of the earth crust (3 °C/100 m). These values are consistent with the thermal anomaly described in this area (IGME, 1983) and are associated with the presence of faults with SW–NE orientation, which bring up the deep water contained in the Paleozoic materials.

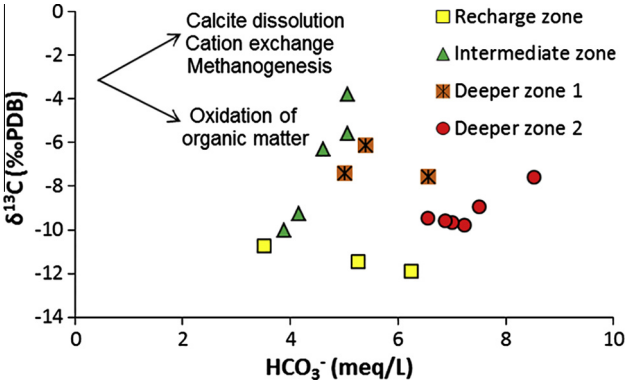

Fig. 8. $\delta^{13}C$ vs. HCO_3 of the groundwater samples analyzed.

The pH values measured ranged between 6.9 and 10.1, and the electrical conductivity (EC) ranged between 607 and 2800 μS/cm, in both cases increasing from NW to SE. The alkalinity shows values between 75 and 427 mg/L $CaCO_3$. Water from the recharge zone is characterized by a high content of dissolved oxygen, with values between 5.5 and 8.7 mg/L. As water moves downgradient becomes depleted in oxygen (<1 mg/L). Following the flow direction, the NP aquifer shows a clear evolution of Ca–HCO_3-type water toward Na–Cl-type water, with intermediate compositions (Na–HCO_3) (Fig. 3).

The Cl/Br molar ratio ($R_{Cl/Br}$) clearly shows two end points, one corresponding to groundwater of the recharge zone ($R_{Cl/Br}$ = 220–550) and the other ($R_{Cl/Br}$ = 640–680) corresponding to deep wells in the Paleozoic. The Cl/Br and Cl/Na relationship shows a mixture between infiltration water and a more saline end member, probably relict syndepositional water trapped in the pores (Figs. 4 and 5). The Cl–Na molar ratio shows that most of the analyses are shifted to higher Na concentrations, indicating the existence of an extra Na source. This is interpreted as the result of cation exchange with the clayish formations with the consequent replacement of Ca by Na in the groundwater (Custodio and Llamas, 1976; Custodio and Bruggeman, 1987; Appelo, 1994). This is a well-known process when pore water in materials deposited in marine environments is slowly replaced by fresh water. The fact that cation exchange is still taking place points to a very slow penetration of continental fresh water into the aquifer.

Saturation indices (SI) were calculated using the PHREEQC code (Appelo and Postma, 2005) with the WATEQ4F thermodynamic database. Most samples are slightly supersaturated in calcite, with SI values between 0.13 and 0.8, with the exception of the recharge zone. Supersaturation is attributed to CO_2 degasification during sampling. Indeed, this is more evident in samples collected from a high pumping rate (>10 L/s). Gas bubbles appeared when the bottle was opened in the laboratory. By re-equilibrating the analyses with calcite, the final P_{CO2} calculated with PHREEQC varies between $10^{-3.3}$ atm and $10^{-1.2}$ atm, and the new recalculated pH values decreased between 0.3 and 0.7 units.

4.2. Stable isotopes

4.2.1. Water isotopes

Groundwater samples show isotopic contents ranging from −21.5‰ to −30.0‰ for δ^2H and −2.9‰ to −5.2‰ for $\delta^{18}O$ (V-SMOW). As shown in Fig. 6, the values follow the Global Meteoric Water Line (GMWL; Craig (1961)), indicating recharge by rainwater infiltration. The samples that correspond to the recharge area (NW) show heavier $\delta^{18}O$ and δ^2H values when compared to samples taken further south. The coincidence of depleted δ^2H and $\delta^{18}O$ values with longer residence times (see below) suggests that the recharge of these samples could have occurred in colder climates than recent samples. The $\delta^{18}O$ and δ^2H values show a positive correlation with the temperature with a slope of 0.69‰ per °C for $\delta^{18}O$ and 5.6‰ per °C for δ^2H (Dansgaard (1964) and Odezulu (2011)). From this information, it can be inferred that the groundwater of the deep zone was recharged under a climate between 1.5 and 3 °C colder than the current annual average temperature. The excess of deuterium, defined by $d = \delta^2H - 8\ \delta^{18}O$ (Dansgaard, 1964), varies between 9.5‰ and 11.6 ‰. These values are close to 10‰ and suggest an Atlantic origin and are consistent with those registered in Doñana National Park (d = 10.9 ± 3.1)

Table 1
Theoretical variation of the concentration of DIC (C in mol/L) involved in the different geochemical processes. Values of $\delta^{13}C$ calculated and $\delta^{13}C$ measured (‰).

Sample	C_{soil}	$C_{calcite}$	$C_{exchange}$	C_{SO4}	C_{Fe}	C_{total}	$\delta^{13}C$ calculated (‰)	$\delta^{13}C$ measured (‰)
Recharge zone								
1	1.50E−03	1.67E−03	–	–	–	3.17E−03	−10.88	−10.73
2	2.70E−03	2.74E−03	–	–	–	5.44E−03	−11.41	−11.52
3	2.00E−03	2.82E−03	–	–	–	4.82E−03	−9.55	–
4	2.00E−03	3.04E−03	–	–	–	5.04E−03	−9.13	–
5	1.71E−03	2.54E−03	–	–	–	4.25E−03	−9.25	–
Intermediate zone								
6	1.90E−03	2.49E−03	2.32E−05	–	–	4.41E−03	−9.95	–
7	1.90E−03	1.81E−03	1.88E−04	–	–	3.90E−03	−11.78	−10.02
8	1.90E−03	1.57E−03	5.66E−04	–	–	4.04E−03	−10.82	−9.26
9	1.90E−03	1.28E−03	5.20E−04	–	–	3.70E−03	−11.83	−3.80
10	1.90E−03	1.73E−03	9.60E−04	–	–	4.59E−03	−9.51	−6.30
11	1.90E−03	1.22E−03	1.06E−03	–	–	4.18E−03	−10.44	−5.57
Deep zone 1								
12	1.90E−03	5.18E−05	2.58E−03	5.18E−04	8.95E−07	5.05E−03	−11.42	−6.16
13	1.90E−03	6.55E−05	2.59E−03	4.96E−04	8.95E−07	5.05E−03	−11.31	−7.44
14	1.90E−03	2.48E−05	4.27E−03	4.24E−04	8.95E−07	6.62E−03	−8.33	–
15	1.90E−03	2.43E−05	3.44E−03	4.52E−04	8.95E−07	5.82E−03	−9.61	−7.57
16	1.90E−03	7.43E−05	3.87E−03	5.97E−04	8.95E−07	6.44E−03	−9.29	–
17	1.90E−03	3.69E−05	3.64E−03	4.74E−04	8.95E−07	6.05E−03	−9.34	–
18	1.90E−03	6.06E−05	3.47E−03	6.38E−04	8.95E−07	6.07E−03	−10.04	–
19	1.90E−03	2.31E−03	2.39E−03	0.00E+00	8.95E−07	6.60E−03	−6.63	–
Deep zone 2								
20	1.90E−03	2.58E−04	4.25E−03	6.38E−04	8.95E−07	7.05E−03	−8.62	−9.65
21	1.90E−03	2.86E−04	4.71E−03	6.38E−04	8.95E−07	7.53E−03	−8.06	−9.59
22	1.90E−03	1.74E−03	2.28E−03	6.38E−04	3.98E−06	6.56E−03	−9.18	−9.47
23	1.90E−03	4.76E−04	3.71E−03	6.38E−04	8.95E−07	6.72E−03	−9.06	−9.79
24	1.90E−03	9.47E−05	4.48E−03	6.38E−04	8.95E−07	7.11E−03	−8.52	−8.94
25	1.90E−03	9.20E−05	4.98E−03	6.38E−04	8.95E−07	7.61E−03	−7.97	−7.58

(Iglesias, 1999; Jimenez and Custodio, 2008). There is a trend to lower d (<10‰) for the fresher waters toward higher *d* (>10‰) as salinity increases. This may reflect different atmospheric conditions of recharge (colder climate with dryer air) for the more saline water (Fig. 6).

4.2.2. Sulfate isotopes

The isotope values of the S and O of the sulfate molecule have been determined in 24 samples. The ^{34}S range between −17.2‰ and 20.4‰ (CDT), and the ^{18}O values between 3.7‰ and 16.9‰ (V-SMOW).

Sulfate isotope values also show a distinct variation from the recharge to the deep zones. Samples in the recharge area have low $\delta^{18}O$ values and a wide range of $\delta^{34}S$ values (Fig. 7). This is compatible with oxidation of sulfides either in granites or in massive sulfide deposits, or with its dispersal in sedimentary materials. The range of $\delta^{18}O_{SO4}$ values obtained in the recharge zone is compatible with $\delta^{18}O_{SO4}$ values of atmospheric sulfates (Mook, 2002). Thus, the $\delta^{34}S$ values obtained are consistent with those between −15‰ and 10‰ reported for the Iberian Pyrite Belt (Sáez et al., 1999). The contribution of other sulfate sources such as those contained in fertilizers or sewage are clearly ruled out.

Samples from the intermediate and especially from the deep zones show a distinct trend toward heavier values of sulfate $\delta^{18}O$ and $\delta^{34}S$ (Fig. 7), thus indicating a sulfate-reduction processes. Thode and Monster (1970) demonstrated that sulfur and sulfides originated by biological sulfate reduction are characterized by heavier isotopic values, following slopes between 0.22 and 0.28 in a plot of $\delta^{18}O$ vs. $\delta^{34}S$. Sulfate-reduction is consistent with clear depletion of sulfate concentration in samples from intermediate and deep zones.

4.2.3. Carbon isotopes

Seventeen samples have been analyzed for $\delta^{13}C$ of dissolved inorganic carbon (DIC). Values increase from −11.5‰ (V-PDB) in the recharge zone to −3.8‰ in the intermediate zone and decrease again to −9.8‰ in the deep zone. This variation is attributed to inorganic C from water–rock reactions that must be quantitatively assessed to correct the ^{14}C values for subsequent dating (Fig. 8).

Theoretical values are calculated and compared with the analytical value from a hypothetical recharge, considering the water–rock reactions described above, according to Coetsiers and Walraevens (2009):

$$\partial^{13}C_{calculated} = \frac{C_{recharge}(-23‰) + C_{calcite}(0‰) + C_{exchange}(0‰) + C_{Fe}(-27‰) + C_{SO4}(-27‰)}{C_{total}} \quad (1)$$

C_{soil}: *C* concentration resulting from CO_2 dissolution and bicarbonate speciation.
$C_{calcite}$: *C* concentration resulting from calcite dissolution.
$C_{exchange}$: *C* concentration resulting from additional calcite dissolution as a result of cation exchange.
C_{Fe}: *C* concentration resulting from Fe(III) reduction.
C_{SO4}: *C* concentration resulting from SO_4 reduction.
C_{total}: the *C* sum of concentration from all above processes.

It is assumed that soil water initially contains DIC derived from atmospheric CO_2. The photosynthetic activity of C3 type plants generates $\delta^{13}C$ values of approximately −27‰ in vegetal matter (Vogel, 1993). When this process overwhelms atmospheric CO_2 diffusion, the respiration of C3 type plants increases the average value of $\delta^{13}C$ in soil CO_2 to −23‰ (Cerling et al., 1991). A theoretical value of the soil carbon (C_{SOIL}) concentration was computed from the chemical composition of the samples located in the recharge zone, eliminating the dissolution of calcite. It accounted for the Ca concentration (inverse modeling). Thus, C_{SOIL} values between 0.0015 and 0.0027 mol/L were obtained for the samples of the recharge zone (Table 1). Then, C_{SOIL} concentration of 0.0019 mol/L, the average value of the range obtained in the recharge zone, was assumed for the intermediate and deep zones.

Following the flow line toward the SE, $\delta^{13}C$ becomes enriched. This fact is related to the strong increase of inorganic carbon from the dissolution of carbonate rocks ($\delta^{13}C \approx 0‰$ for marine carbonates). The $C_{calcite}$ value was calculated from the amount of Ca measured in water and is attributed to calcite dissolution according to the stoichiometry of Eq. (2). This dissolution is enhanced by the Ca–Na cation exchange that occurs in the clay materials, causing high calcium consumption. The calcite dissolution because of cation exchange was calculated from the excess of Na^+ with respect to the theoretical fresh-seawater mixing line (Fig. 5) and the molal stoichiometry of Eqs. (2) and (3).

$$CaCO_3 + H^+ \rightarrow Ca^{2+} + HCO_3^- \quad (2)$$

$$Ca^{2+} + 2X - Na \rightarrow X_2 - Ca + 2Na^+ \quad (3)$$

The oxidation of organic matter provides dissolved inorganic carbon to groundwater that must also be taken into account. Thus, the analysis of dissolved H_2S (0.095–0.113 mg/L), the SO_4 depletion and the $\delta S_{SO4} - \delta^{18}O_{SO4}$ clearly indicate the existence of sulfate reduction process.

$$2CH_2O + SO_4^{-2} \rightarrow H_2S + 2HCO_3^- \quad (4)$$

The carbon resulting from SO_4 reduction was computed from the loss of SO_4 concentration with respect to the recharge value and the stoichiometry of reaction (4). The SO_4 concentration in the recharge water was estimated as the average concentration in the samples from the recharge zone ($C_{SO4} = 4 \cdot 10^{-4}$ mol/L).

$$2CH_2O + 4FeOOH + 7H^+ \rightarrow 4Fe^{+2} + HCO_3^- + 6H_2O \quad (5)$$

Dissolved organic matter (DOC) can also be oxidized by Fe(III) oxides present in the host rocks according to reaction (5). The inorganic carbon generated (C_{Fe}) could be computed from the Fe(II) dissolved in water. However, the Fe(II) concentration is always below the detection limit ($4 \cdot 10^{-4}$ mol/L). Low Fe(II) concentrations in water could be due to the precipitation of Fe(II) phases such as Fe sulfides and carbonates. Indeed, siderite and small amounts of pyrite are described to replace Fe-oxides extensively. The Cobre Las Cruces ore deposit is a unique mineralization, where initial Fe-oxides of the gossan are replaced by siderite from Miocene to recent times (Yesares et al., 2014). Consistently, the Fe(II) concentration predicted in water in equilibrium with siderite is below the detection level in all samples. Therefore, the HCO_3^- originating from organic matter oxidation by FeOOH reduction is not computed. Consequently, the final $\delta^{13}C$ resulting from calculations will be overestimated.

The production of CH_4 from existing organic matter is another process that can potentially increase the $\delta^{13}C$ values of groundwater dissolved carbon (Coetsiers and Walraevens, 2009). However, CH_4 concentrations were below the detection limit (0.58 mg/L) for all samples. Therefore, methanogenesis has not been incorporated as a process modifying the $\delta^{13}C$ of residual dissolved inorganic carbon.

Applying Eq. (1), the $\delta^{13}C$ is calculated and incorporates all carbon contribution from each chemical processes identified. Calculated and measured $\delta^{13}C$ are similar in recharge, deep 1 and deep 2 groundwaters. However, some samples located in the intermediate and deep zone 1 calculations result in $\delta^{13}C$ values distinctly more depleted (Table 1). Several hypotheses to account for these differences have been considered: (1) Additional calcite dissolution triggered by Ca exchange by Sr and Mg. The unusually high concentrations of Mg^{2+} and Sr^{2+} in this groundwater suggest this process could be viable. Incorporation of this process into the carbon mass balance improves the calculated $\delta^{13}C$ but not enough to explain the observed differences. (2) Dissolution of gypsum intercalations. This would explain the increase of SO_4^{2-} concentrations observed in these samples; however, this would also produce an increase in Ca^{2+} concentration leading to precipitation of $CaCO_3$. This hypothesis can be ruled out, as this would be accompanied by a decrease of HCO_3^- that was not observed. (3) Sample degassing during sampling. This was observed, particularly for those wells extracted with a high flow (10 L/s) pump. It is believed that the sample could not be equilibrated with atmospheric CO_2 during the sampling and the opening of the bottle in the laboratory produced sample degassing. The CO_2 degassing would cause isotopic fractionation in the HCO_3^-–CO_2 system and, consequently, the sample would be enriched (Wendt, 1968). The $\delta^{13}C$ value considering this isotopic fractionation was calculated as:

$$\delta^{13}C_i * X_i = \delta^{13}C_f * X_f + \delta^{13}C_{CO_2} * X_{CO_2} \quad (6)$$

where,

X_i, X_f and X_{CO_2} are, respectively, the initial, final and CO_2 molar concentration.

$\delta^{13}C_i$ and $\delta^{13}C_f$ are the initial and final $\delta^{13}C$ values of HCO_3.

$\delta^{13}Cco_2$ is the CO_2 isotopic composition. This value depends on the temperature and is calculated from the expression of Mook et al. (1974) for the isotopic fractionation $\varepsilon_{CO2/HCO3}$:

$$^{13}\varepsilon_{CO2/HCO3} = -9483/T + 23.89‰ \quad (7)$$

These calculations lead to $\delta^{13}C$ values with a maximum enrichment of 2‰, but not high enough to match the analyses.

Therefore, a consistent explanation for the anomalous $\delta^{13}C$ values measured in these samples has not been found.

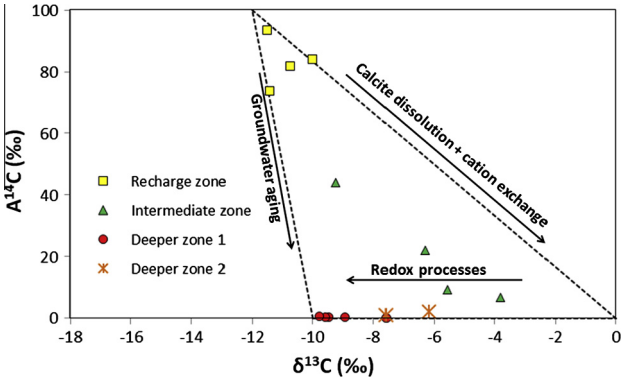

Fig. 9. $A^{14}C$ vs. $\delta^{13}C$.

4.3. Groundwater residence time

4.3.1. Tritium (^3H) in groundwater

The evolution of the tritium activity in rainfall in the area over the last 50 years is recorded from the values registered at the Global Network of Isotopes in Precipitation (GNIP) Gibraltar station. Assuming a piston flow model, the activity (A) for every year is calculated and then compared to groundwater activity obtained analytically.

The tritium concentrations in precipitation near the study area in the past 50 years are over 3 TU, with a maximum of 597 TU for 1963, which corresponds to maximum of atmospheric nuclear bomb tests that took place during that time. If these tritium concentrations are corrected for radioactive decay, some of this tritium could be found in the actual concentration in recent groundwater (Custodio and Custodio-Ayala, 2013). Tritium content in current rainfall is close to natural values since a few years ago, with some small influence of the small increase in the ocean and the possible influence of evaporating recent groundwater in irrigated fields.

Table 2
Dating of groundwater by ^{14}C with Tamers and Pearson correction (ky). The Pearson correction is calculated from $\delta^{13}C$ measured and $\delta^{13}C$ calculated.

Samples	Activity (pmC)	$\delta^{13}C_{MEASURED}$ (‰)	$\delta^{13}C_{CALCULATED}$ (‰)	Tamers (ky)	Pearson (ky) from $\delta^{13}C_{MEASURED}$ (‰)	Pearson (ky) from $\delta^{13}C_{CALCULATED}$ (‰)
Recharge zone						
2	84.17	−10.02	−11.78	MODERN (<0.06)	MODERN (<0.06)	MODERN (<0.06)
1	93.52	−11.52	−11.41	MODERN (<0.06)	MODERN (<0.06)	MODERN (<0.06)
Intermediate zone						
7	81.89	−10.73	−10.88	MODERN (<0.06)	MODERN (<0.06)	MODERN (<0.06)
8	43.98	−9.26	−10.82	2	–	1
10	21.97	−6.3	−9.51	8	2	6
9	6.7	−3.8	−11.83	17	8	17
11	9.2	−5.57	−10.44	14	9	14
Deep zone 1						
12	1.95	−6.16	−11.42	27	22	27
15	0.87	−7.57	−9.61	>30	>30	>30
Deep zone 2						
23	0.65	−9.79	−9.06	>30	>30	>30
22	0.44	−9.47	−9.18	>30	>30	>30
24	0.34	−8.94	−8.52	>30	>30	>30
21	0.32	−9.59	−8.06	>30	>30	>30
25	0.17	−7.58	−7.97	>30	>30	>30

Table 3
^{36}Cl values obtained from 7 groundwater samples and estimation of their apparent age (ky).

Samples	Cl (mg/L)	$^{36}Cl/Cl$ ($\times 10^{-15}$)	Apparent age (ky)
12	199	35.9 ± 2.1	41
15	97	36.7 ± 2.2	28
23	598	31.4 ± 1.9	124
22	1349	30.5 ± 1.9	142
24	472	30.7 ± 1.9	138
21	571	25.3 ± 1.7	269
25	428	31.8 ± 2.0	116

Tritium was measured in 9 groundwater samples from wells of different depths and screened in both the NP and the Paleozoic. Tritium activity in groundwater ranged from 2 TU in the recharge zone to less than the quantification limit (0.3 TU) in the rest of the studied area. Therefore, the tritium values registered in the recharge zone indicate that most of this water was recharged after 1952. However, the null tritium values of the rest of the study area indicate that the water recharge was produced prior to 1952.

4.3.2. ^{14}C Isotope in groundwater

A decrease in the ^{14}C activity is observed along the carbonate dissolution and cation exchange line, as well as an increase in the $\delta^{13}C$ values (Fig. 9). There is a line marked by redox processes where the ^{14}C activity is close to 0 and $\delta^{13}C$ values tend to decrease. Finally, there is a line that represents the aging groundwater where the ^{14}C activity decreased and the $\delta^{13}C$ values remain more or less constant. Following a flow line: (1) the composition of the samples of the intermediate zone is dominated by the processes of dissolution of carbonate rocks and cation exchange. (2) The deep zones exhibit low ^{14}C activity and $\delta^{13}C$ values are lightest due to the dominance of the redox reactions.

The activity of ^{14}C of 14 groundwater samples decreases downgradient along a NW–SE flow line. Activities range from 93 pMC to <1 pMC (Table 2), with three different ranges that broadly correspond to the groundwater zones. These ranges are differentiated as follows: (1) values between 93 and 84 pMC in the recharge zone; (2) values from 82 to 9 pMC in the intermediate zone; and (3) activities lower than 2 pMC found in the deep saline waters to the SE of the study area.

Assuming a piston flow, the ^{14}C age is calculated from the following equation:

$$t = \frac{\ln \frac{A}{q^* A_0}}{-\lambda}$$

where A is the measured ^{14}C activity, q is the dilution factor, A_0 is the initial ^{14}C concentration and λ is the decay constant ($\lambda = \ln 2/t_{1/2}$), $t_{1/2}$ being the half-life.

The value of the initial concentration of ^{14}C (A_0) is affected by the processes that modify the C content in the water, as explained in the discussion of ^{13}C. The dominant processes are the dissolution of carbonate rocks and organic matter oxidation. During the transit in the aquifer, these processes modify the initial ^{14}C content in groundwater because the ancient rocks do not contain ^{14}C. Hence, a correction must be applied to better approximate the A_0 value in carbonate rich aquifers. Here, the chemical correction (Tamers, 1975) and the isotopic correction (Pearson, 1965) in their simpler forms are considered.

The dating of these waters using both corrections (Tamers and Pearson) is in Table 2. The measured and calculated $\delta^{13}C$ values have been used for the Pearson correction. In the intermediate zone, significant differences in age are obtained between the two types of corrections. Samples that show these differences are those that have inconsistencies between the $\delta^{13}C_{CALCULATED}$ and the $\delta^{13}C_{MEASURED}$ values, as already mentioned in Carbon Isotopes section. The Pearson correction using the $\delta^{13}C_{CALCULATED}$ values results in ages very close to those from the Tamers correction. Therefore, age data use the Tamers correction because it is independent of the $\delta^{13}C$ values.

Four zones can be distinguished: (1) recent water area (<0.06 ky) where the values calculated of ^{14}C coincide with significant values of tritium and consequently affected by post-nuclear recharge; (2) water of intermediate age area (0.06–20 ky); (3) old water (20–30 ky); and (4) very old water (>30 ky).

4.3.3. ^{36}Cl Isotopes in groundwater

Seven groundwater samples have been analyzed, mostly selected from the deeper zone and expected to have ages beyond ^{14}C dating range. While the ideal range for ^{36}Cl is for samples between ~40 ky and 3000 ky (Fabryka Martin et al., 1987), there are important limitations to be considered: (1) variable input of the $^{36}Cl/Cl$ ratio through time and under prevalent climatic conditions.; (2) in-situ ^{36}Cl production by secular equilibrium with formation rocks; and (3) mixing of waters with different ^{36}Cl (Kulongoski et al., 2008). The modern local rainfall weighted $^{36}Cl/Cl$ values in

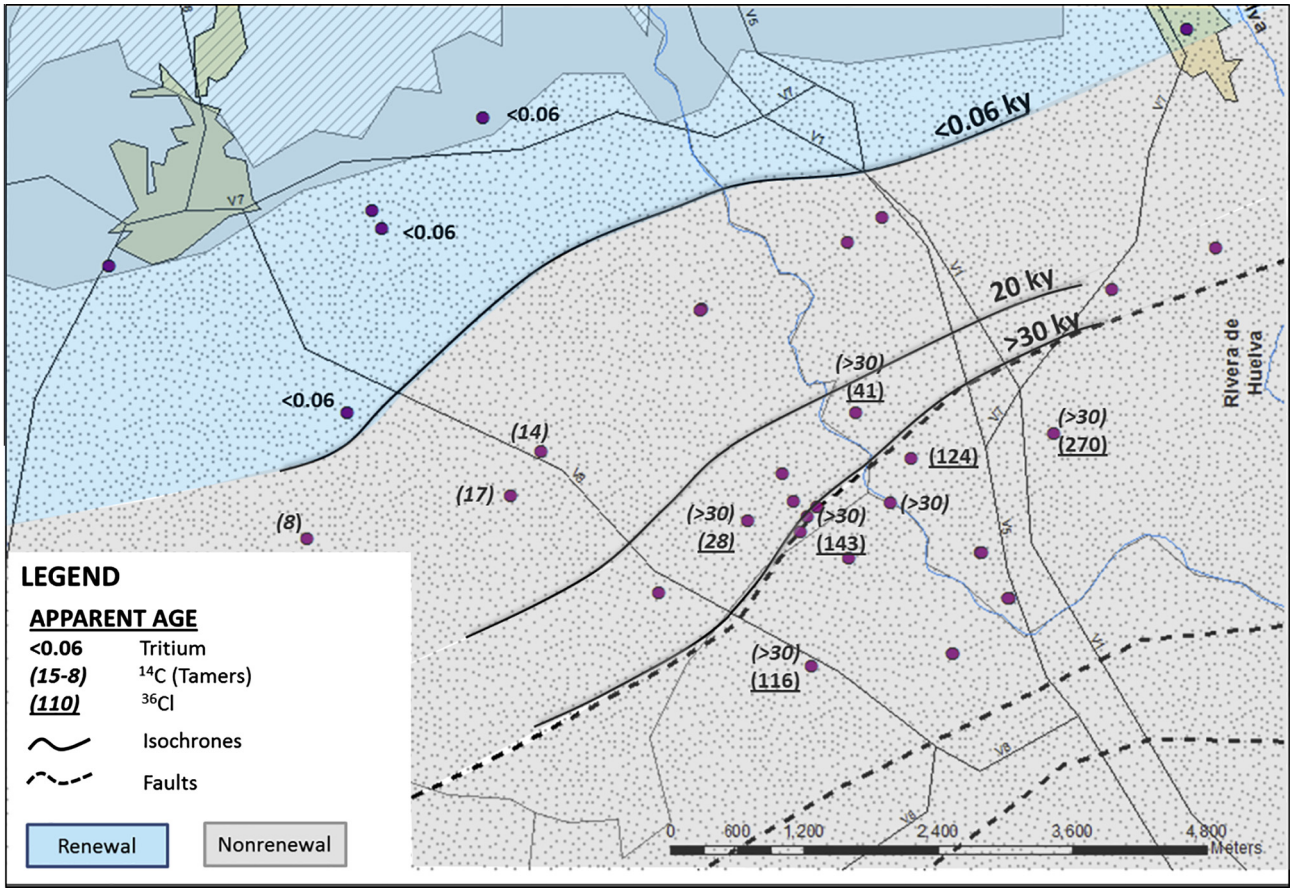

Fig. 10. Map of groundwater dating (ky) from ^{3}H, ^{14}C (Tamers) and ^{36}Cl. Zoning of renewable and nonrenewable resources.

Seville, are estimated to be $27x10^{-15}$ and are affected by the arrival of dead (no ^{36}Cl) chloride from the sea (Santos et al., 2004).

Evapotranspiration effects during recharge are expected to modify further the $^{36}Cl/Cl$ of recharge; however, these cannot be quantified. All of these combined effects make the estimation of the initial $^{36}Cl/Cl$ of recharge to groundwater problematic, particularly for samples with Cl^- concentration higher than 75–150 mg/kg (Park et al., 2002). However, for sake of simplicity, a simple piston flow regime is assumed to estimate ^{36}Cl residence times. It is a valid concept if it is considered that no significant contribution to the NW of NP aquifer (from recharge to deep zone 1) comes from the Paleozoic basement. In this case, it has been used in the model of Bentley et al. (1986):

$$t = \frac{-1}{\lambda_{36}} \ln \frac{R - R_{se}}{R_0 - R_{se}}$$

where R is the $^{36}Cl/Cl$ ratio measured in the sample, R_0 is the $^{36}Cl/Cl$ initial relationship or meteoric water, and R_{se} is the $^{36}Cl/Cl$ relationship under secular equilibrium with the materials that form in this case the NP aquifer.

A value of 38 ($\times 10^{-15}$) has been selected as an initial ratio $^{36}Cl/Cl$ (R_0), which is slightly greater than the average value (32×10^{-15}). According to Fabryka Martin et al. (1987), the relationship $^{36}Cl/Cl$ under secular equilibrium (R_{se}) with Paleozoic materials is 13 ($\times 10^{-15}$); in the Cenozoic materials it is 5 ($\times 10^{-15}$). An intermediate value of 10 ($\times 10^{-15}$) has been selected for the NP aquifer.

An apparent age of approximately 30 ky has been obtained for the younger waters, consistent with that obtained from ^{14}C, and from 100 to 150 ky for the rest of the deep zone areas (Table 3). However, most of the samples have a Cl concentration greater than 150 mg/L. Therefore, the ages obtained are probably an overestimation.

5. Conclusions

The study area was divided into four zones: recharge, intermediate, and deep (1 and 2) zones. This zonation corresponds to geochemical and isotopic differences and correlate with the primary geological features.

The groundwater from the NP aquifer shows a clear evolution of Ca–HCO3-type water toward Na-Cl-type water. The origin of the salinity in the samples collected in the deep areas can be explained by the Na/Cl and Br/Cl ionic relationships. Both relationships suggest a mixture of fresh water with a more saline end member, probably relict syndepositional water trapped in the pores.

Sulfate isotope values indicate the existence of oxidation of sulfides processes in the recharge zone and sulfate-reduction processes in the deep zones.

The ^{13}C isotope values have facilitated identification of hydrogeochemical processes occurring in the NP aquifer: calcite dissolution, Ca–Na cation exchange, SO_4^{2-} and iron oxide reduction. Knowing the processes taking place in each area, enabled to carry out a correction of $\delta^{13}C$ values of each of the sampled points. This correction has improved the results of ^{14}C dating of the groundwater.

Based on the results obtained from isotopic data, ^{3}H, ^{14}C and ^{36}Cl, four age zones can be established in the study area from NW to SE (Fig. 10). The first zone corresponds to young waters (<0.06 ky); it has been defined using tritium dating and corresponds to the recharge area. The second (0.06–20 ky) and

third zones (20–30 ky) correspond to the intermediate and deep zone 1, respectively; both zones have been defined with ^{14}C values and confirmed by ^{36}Cl dating results. The fourth zone (>30 ky) corresponds to very old water of deep zone 2, with residence times of thousands of years. This was dated using ^{36}Cl, although the high Cl content makes precise dating difficult.

However, relatively high differences in age can be distinguished along the flow. Thus, age gradients appear to be highly conditioned by the local geology. The >30 isochrone coincides with a SW–NE regional fault that constitutes one of the main areas of the Paleozoic aquifer discharge. Discharge zones are very difficult to unravel in such deep aquifers and, therefore, groundwater ages can be an indirect way to infer such deep flow paths.

From the results obtained, particularly with radioactive isotopes, a strip zone with short turnover time (renewable) groundwater and another with almost steady (nonrenewable) groundwater are distinguished (Fig. 10). Therefore, anyone acting in the area defined as almost steady must consider this aspect to ensure the sustainability of these groundwater resources that are probably nonrenewable due to the slow transfer from the renewable area. Then any extraction of water resources, such as draining operations in a mine, must reset the water pressures by artificial recharge to avoid affecting the area defined as renewable water. Other considerations refer the possible poor water quality, which are not addressed here.

Acknowledgements

This work has been supported by Fundación Migres. Other financial support was provided by the Spanish Government project CGL2013-48460-C2-R. We are also grateful to the staff of Cobre Las Cruces for their collaboration during of fieldwork and granting access to the mine. We wish to thanks Dr. Manuela Barbieri for fieldwork and laboratory assistance, and Chris Dimovski and Alan Williams (ANSTO) for their help with ^{14}C sample preparation and logistics.

Appendix A. Supplementary material

Supplementary data associated with this article can be found, in the online version, at http://dx.doi.org/10.1016/j.jhydrol.2015.01.076.

References

Alcalá, F.J., Custodio, E., 2008. Using the Cl/Br ratio as a tracer to identify the origin of salinity in aquifers in Spain and Portugal. J. Hydrol. 359 (1–2), 189–207.
Andre, L., Franceschi, A., Pouchan, P., Atteia, O., 2005. Using geochemical data and modelling to enhance the understanding of groundwater flow in a regional deep aquifer, Aquitaine Basin, south-west of France. J. Hydrol. 305 (1-4), 40–62.
Appelo, C.A.J., 1994. Cation and proton exchange, pH variations, and carbonate reactions in a freshening aquifer. Water Resour. Res. 30 (10), 2793–2805.
Appelo, C.A.J., Postma, D., 2005. Geochemistry, groundwater and pollution (Second Edition). CRC Press, 1–668.
Atkinson, A.P., Cartwright, I., Gilfedder, B.S., Hofmann, H., Unland, N.P., Cendón, D.I., Chisari, R., 2013. A multi-tracer approach to quantifying groundwater inflows to an upland river; assessing the influence of variable groundwater chemistry. Hydrol. Process. http://dx.doi.org/10.1002/hyp.10122.
Bentley, H.W., Phillips, F.M., Davis, S.N., Habermehl, M.A., Airey, P.L., Calf, G.E., Elmore, D., Gove, H.E., Torgersen, T., 1986. Chlorine 36 dating of very old groundwater: 1. The Great Artesian Basin, Australia. Water Resour. Res. 22 (13), 1991–2001.
Blake, C., 2008. The mineralogical characterization and interpretation of a precious metal-bearing fossil gossan, Las Cruces, Spain., Cardiff University: 330 pp.
Bouchaou, L., Michelot, J.L., Vengosh, A., Hissou, Y., Qurtobi, M., Gaye, C.B., Bullen, T.D., Zuppi, G.M., 2008. Application of multiple isotopic and geochemical tracers for investigation of recharge, salinization, and residence time of water in the Souss-Massa aquifer, southwest of Morocco. J. Hydrol. 352 (3–4), 267–287.
Capasso, G., Inguaggiato, S., 1998. A simple method for the determination of dissolved gases in natural waters. An application to thermal waters from Vulcano Island. Appl. Geochem. 13 (5), 631–642.
Capitán Suárez, M.A., 2006. Mineralogía y geoquímica de la alteración superficial de depósitos de sulfuros masivos en la faja pirítica ibèrica. Departamento de geología, Universidad de Huelva (UHU): 368.
Cartwright, I., Weaver, T., Cendón, D.I., Swane, I., 2010. Environmental isotopes as indicators of inter-aquifer mixing, Wimmera region, Murray Basin, Southeast Australia. Chem. Geol. 277 (3–4), 214–226.
Cartwright, I., Weaver, T.R., Cendón, D.I., Fifield, L.K., Tweed, S.O., Petrides, B., Swane, I., 2012. Constraining groundwater flow, residence times, inter-aquifer mixing, and aquifer properties using environmental isotopes in the southeast Murray Basin, Australia. Appl. Geochem. 27 (9), 1698–1709.
Cendón, D.I., Hankin, S.I., Williams, J.P., Van der Ley, M., Peterson, M., Hughes, C.E., Meredith, K., Graham, I.T., Hollins, S.E., Levchenko, V., Chisari, R., 2014. Groundwater residence time in a dissected and weathered sandstone plateau: Kulnura-Mangrove Mountain aquifer, NSW, Australia. Aust. J. Earth Sci. 61 (3), 475–499.
Cerling, T.E., Solomon, D.K., Quade, J., Bowman, J.R., 1991. On the isotopic composition of carbon in soil carbon dioxide. Geochim. Cosmochim. Acta 55 (11), 3403–3405.
CHG, 2012. Propuesta de Proyecto de Plan Hidrológico de la Demarcación Hidrográfica del Guadalquivir. Sevilla.
Cloutier, V., Lefebvre, R., Savard, M., Bourque, É., Therrien, R., 2006. Hydrogeochemistry and groundwater origin of the Basses-Laurentides sedimentary rock aquifer system, St. Lawrence Lowlands, Québec, Canada. Hydrogeol. J. 14 (4), 573–590.
Coetsiers, M., Walraevens, K., 2009. A new correction model for ^{14}C ages in aquifers with complex geochemistry – Application to the Neogene Aquifer, Belgium. Appl. Geochem. 24 (5), 768–776.
Craig, H., 1961. Isotopic variations in meteoric waters. Science 133 (346), 1702–1703.
Cresswell, R.G., Bauld, J., Jacobson, G., Khadka, M.S., Jha, M.G., Shrestha, M.P., Regmi, S., 2001. A first estimate of ground water ages for the deep aquifer of the Kathmandu Basin, Nepal, using the radioisotope chlorine-36. Ground Water 39 (3), 449–457.
Currell, M., Cendón, D., Cheng, X., 2013. Analysis of environmental isotopes in groundwater to understand the response of a vulnerable coastal aquifer to pumping: Western Port Basin, south-eastern Australia. Hydrogeol. J. 21 (7), 1413–1427.
Custodio, E., Bruggeman, G.A., 1987. Groundwater problems in coastal areas. Studies & Reports in Hydrology 45. UNESCO, Paris: pp. 1–576.
Custodio, E., Custodio-Ayala, J., 2013. Interpretación simplificada de la evolución del tritio en acuíferos con mezcla exponencial [Symplified interpretation of tritium evolution in aquifers with exponential mixing]. In: X Simposio de Hidrogeología, Granada, Hidrogeología y Recursos Hidráulicos. Asociación Española de Hidrogeólogos, Madrid, XXX: pp. 427–436.
Custodio, E., Llamas M.R. (Eds.) 1976. Hidrología subterránea [Groundwater hydrology]. Ediciones Omega, Barcelona: pp. 1–2350.
Dansgaard, W., 1964. Stable isotopes in precipitation. Tellus 16 (4), 436–468.
Davis, S.N., Whittemore, D.O., Fabryka-Martin, J., 1998. Uses of chloride/bromide ratios in studies of potable water. Ground Water 36 (2), 338–350.
Dogramaci, S.S., Herczeg, A.L., 2002. Strontium and carbon isotope constraints on carbonate-solution interactions and inter-aquifer mixing in groundwaters of the semi-arid Murray Basin, Australia. J. Hydrol. 262 (1–4), 50–67.
Douglas, A.A., Osiensky, J.L., Keller, C.K., 2007. Carbon-14 dating of ground water in the Palouse Basin of the Columbia river basalts. J. Hydrol. 334 (3–4), 502–512.
Edmunds, W.M., 2009. Palaeoclimate and groundwater evolution in Africa-implications for adaptation and management. Hydrol. Sci. J.-J. des Sci. Hydrolog. 54 (4), 781–792.
Edmunds, W., Fellman, E., Goni, I., Prudhomme, C., 2002. Spatial and temporal distribution of groundwater recharge in northern Nigeria. Hydrogeol. J. 10 (1), 205–215.
Fabryka Martin, J., Davis, S.N., Elmore, D., 1987. Applications of ^{129}I and ^{36}Cl in hydrology. Nucl. Instrum. Methods Phys. Res., Sect. B 29 (1–2), 361–371.
Fernández-Caliani, J.C., Galán, E., 1991. Las pizarras de la faja piritica Ibérica (zona sur-Portuguesa): geología, mineralogía y aplicaciones industriales. Estud. Geol. 47 (5–6), 1991. http://dx.doi.org/10.3989/egeol.91475-6425.
Fifield, L.K., Ophel, T.R., Bird, J.R., Calf, G.E., Allison, G.B., Chivas, A.R., 1987. The chlorine-36 measurement program at the Australian National University. Nucl. Instrum. Methods Phys. Res., Sect. B 29 (1–2), 114–119.
Frengstad, B., Banks, D., Siewers, U., 2001. The chemistry of Norwegian groundwaters: IV. The pH-dependence of element concentrations in crystalline bedrock groundwaters. Sci. Total Environ. 277 (1–3), 101–117.
Guendouz, A., Michelot, J.-L., 2006. Chlorine-36 dating of deep groundwater from northern Sahara. J. Hydrol. 328 (3–4), 572–580.
Herrera, C., Custodio, E., 2000. Utilización de la Relación Cl/Br Como Trazador Hidrogeoquímico en Hidrología Subterránea. Boletín Geológico Minero, Madrid.
Iglesias, M., 1999. Caracterización Hidrogeoquímica del Flujo del Agua Subterránea en El Abalario, Doñana. Universidad Politécnica de Cataluña, Huelva.
IGME., 1983. Prospección geotérmica en Andalucía occidental. Instituto Geológico y Minero de España. Madrid (internal report).
Jimenez, D., Custodio, E., 2008. El exceso de deuterio en la lluvia y en la recarga a los acuíferos en el área circum-mediterránea y en la costa mediterránea española [Deuterium excess in rain and recharge to the aquifers in the Circum-Mediterranean área and in the Spanish coastal area]. Boletín Geológico Minero. Madrid. 119, 21–32.
Kulongoski, J.T., Hilton, D.R., Cresswell, R.G., Hostetter, S., Jacobson, G., 2008. Helium-4 characteristics of groundwaters from Central Australia: comparative

chronology with chlorine-36 and carbon-14 dating techniques. J. Hydrol. 348 (1–2), 176–194.
Mahlknecht, J., Garfias-Solis, J., Aravena, R., Tesch, R., 2006. Geochemical and isotopic investigations on groundwater residence time and flow in the Independence Basin, Mexico. J. Hydrol. 324 (1–4), 283–300.
Meredith, K., Cendón, D.I., Pigois, J.-P., Hollins, S., Jacobsen, G., 2012. Using C-14 and H-3 to delineate a recharge 'window' into the Perth Basin aquifers, North Gnangara groundwater system, Western Australia. Sci. Total Environ. 414, 456–469.
Mook, W.G., 2002. Isótopos ambientales en el ciclo hidrológico: principios y aplicaciones. Instituto Geológico y Minero de España, Sevicio de Publicaciones, Serie: Guías y Manuales 1. Madrid: pp. 1–596.
Mook, W.G., Bommerson, J.C., Staverman, W.H., 1974. Carbon isotope fractionation between dissolved bicarbonate and gaseous carbon dioxide. Earth Planet. Sci. Lett. 22 (2), 169–176.
Navarro, A., Fernández, A., Doblas, J.G., 1993. In: IGME (Ed.), Las aguas subterráneas en España. Instituto Geológico y Minero de España: pp. 255–256.
Odezulu, C.I., 2011. Stable hydrogen and oxygen isotopic variations in natural waters in North Florida: implications for hydrological and paleoclimatic studies., University of Florida, Gainesville.
Park, J., Bethke, C.M., Torgersen, T., Johnson, T.M., 2002. Transport modeling applied to the interpretation of groundwater Cl-36 age. Water Resour. Res. 38 (5), 2002, Doi: 0.1029/2001WR000399.
Pearson, F.J., 1965. Use of C-13/C-12 ratios to correct radiocarbon ages of material initially diluted by limestone. In: 6th International Conference Radiocarbon and Tritium Dating, Pulman, Washington.
Plummer, L.N., Eggleston, J.R., Andreasen, D.C., Raffensperger, J.P., Hunt, A.G., Casile, G.C., 2012. Old groundwater in parts of the upper Patapsco aquifer, Atlantic Coastal Plain, Maryland, USA: evidence from radiocarbon, chlorine-36 and helium-4. Hydrogeol. J. 20 (7), 1269–1294.
Sáez, R., Pascual, E., Toscano, M., Almodóvar, G.R., 1999. The Iberian type of volcano-sedimentary massive sulphide deposits. Mineral Deposita 34 (5–6), 549–570.
Santos, F.J., López-Gutiérrez, J.M., García-León, M., Schnabel, C., Synal, H.-A., Suter, M., 2004. Analysis of ^{36}Cl in atmospheric samples from Seville (Spain) by AMS. Nuclear Instruments and Methods in Physics Research Section B: Beam Interactions with Materials and Atoms, 223–22. pp. 501–506. ISSN 0168–583X (doi: http://dx.doi.org/10.1016/j.nimb.2004.04.094).
Stuiver, M., Polach, H.A., 1977. Discussion: reporting of ^{14}C data. Radiocarbon 19 (3), 355–363.
Su, C., Wang, Y., Pan, Y., 2013. Hydrogeochemical and isotopic evidences of the groundwater regime in Datong Basin, Northern China. Environ. Earth Sci. 70 (2), 877–885.
Sukhija, B.S., Reddy, D.V., Nagabhushanam, P., Bhattacharya, S.K., Jani, R.A., Kumar, D., 2006. Characterisation of recharge processes and groundwater flow mechanisms in weathered-fractured granites of Hyderabad (India) using isotopes. Hydrogeol. J. 14 (5), 663–674.
Tamers, M.A., 1975. Validity of radiocarbon dates on ground water. Geophys. Surv. 2 (2), 217–239.
Thode, H.G., Monster, J., 1970. Sulfur isotope abundances and genetic relations of oil accumulations in Middle East basin. Am. Assoc. Pet. Geol. 54, 627–637.
Torres, E., Mix Alan, C., Rugh Williamk D., 2005. Precise δ13C analysis of dissolved inorganic carbon in natural waters using automated headspace sampling and continuous-flow mass spectrometry. Limnol. Oceanogr.: Methods 3.
Tóth, J., 1999. Groundwater as a geologic agent: an overview of the causes, processes, and manifestations. Hydrogeol. J. 7 (1), 1–14.
Vogel, J.C., 1993. 4 – Variability of Carbon Isotope Fractionation during Photosynthesis. In: Bernard, S., James, R.E., Anthony, E.H., Graham D. FarquharA2 – Bernard Saugier, J.R.E.A.E.H., Graham, D.F. (Eds.), Stable Isotopes and Plant Carbon-water Relations. Academic Press, San Diego, pp. 29–46.
Wallin, B., Gaye, C., Gourcy, L., Aggarwal, P., 2005. Isotope methods for management of shared aquifers in northern Africa. Ground Water 43 (5), 744–749.
Wen, X., Wu, Y., Su, J., Zhang, Y., Liu, F., 2005. Hydrochemical characteristics and salinity of groundwater in the Ejina Basin, Northwestern China. Environ. Geol. 48 (6), 665–675.
Wendt, I., 1968. Fractionation of carbon isotopes and its temperature dependence in the system CO2-Gas-CO_2 in solution and HCO3–CO_2 in solution. Earth Planet. Sci. Lett. 4 (1), 64–68.
Whittemore, D.O., 1988. Bromide as a tracer in ground-water studies: geochemistry and analytical determination. Proc. Ground Water Geochem. Conf., Denver National Water Well Assoc. Dublin, Ohio: pp. 339–360.
Yesares, L., Sáez, R., Nieto, J.M., de Almodóvar, G.R., Cooper, S., 2014. Supergene enrichment of precious metals by natural amalgamation in the Las Cruces weathering profile (Iberian Pyrite Belt, SW Spain). Ore Geol. Rev. 58, 14–26.